

A tunable narrow-linewidth Raman laser based on high quality packaged microrod resonator

Cheng-Nian Liu(刘承念), Min Wang(王敏), Song-Yi Liu(刘嵩义), Bing Duan(段冰), Ying-Zhan Yan(严英占), Yu Wu(吴宇), Xiao-Chong Yu(俞骁翀), Bei-Bei Li(李贝贝), and Da-Quan Yang(杨大全)

Citation: Chin. Phys. B, 2025, 34 (**12**): 124203. DOI: 10.1088/1674-1056/adea5a
http://cpb.iphy.ac.cn; http://iopscience.iop.org/cpb

What follows is a list of articles you may be interested in

Gigahertz frequency hopping in an optical phase-locked loop for Raman lasers

Dekai Mao(毛德凯), Hongmian Shui(税鸿冕), Guoling Yin(殷国玲), Peng Peng(彭鹏), Chunwei Wang(王春唯), and Xiaoji Zhou(周小计)

Chin. Phys. B, 2024, 33 (**2**): 024209. DOI: 10.1088/1674-1056/ad174b

Multi-wavelength continuous-wave Nd:YVO_4 self-Raman laser under in-band pumping

Li Fan(樊莉), Xiao-Dong Zhao(赵孝冬), Yun-Chuan Zhang(张蕴川), Xiao-Dong Gu(顾晓东), Hao-Peng Wan(万浩鹏), Hui-Bo Fan(范会博), Jun Zhu(朱骏)

Chin. Phys. B, 2019, 28 (**8**): 084210. DOI: 10.1088/1674-1056/28/8/084210

High-power linearly-polarized tunable Raman fiber laser

Jiaxin Song(宋家鑫), Hanshuo Wu(吴函烁), Jiangming Xu(许将明), Hanwei Zhang(张汉伟), Jun Ye(叶俊), Jian Wu(吴坚), Pu Zhou(周朴)

Chin. Phys. B, 2018, 27 (**9**): 094209. DOI: 10.1088/1674-1056/27/9/094209

An efficient continuous-wave YVO_4/Nd: YVO_4/YVO_4 self-Raman laser pumped by a wavelength-locked 878.9 nm laser diode

Li Fan(樊莉), Weiqian Zhao(赵伟倩), Xin Qiao(乔鑫), Changquan Xia(夏长权), Lichun Wang(汪丽春), Huibo Fan(范会博), Mingya Shen(沈明亚)

Chin. Phys. B, 2016, 25 (**11**): 114207. DOI: 10.1088/1674-1056/25/11/114207

Backward Raman amplification in plasmas with chirped wideband pump and seed pulses

Wu Zhao-Hui (吴朝辉), Wei Xiao-Feng (魏晓峰), Zuo Yan-Lei (左言磊), Liu Lan-Qin (刘兰琴), Zhang Zhi-Meng (张智猛), Li Min (李敏), Zhou Yu-Liang (周煜梁), Su Jing-Qin (粟敬钦)

Chin. Phys. B, 2015, 24 (**1**): 014211. DOI: 10.1088/1674-1056/24/1/014211

A tunable narrow-linewidth Raman laser based on high quality packaged microrod resonator

Cheng-Nian Liu(刘承念)[1,2], Min Wang(王敏)[3], Song-Yi Liu(刘嵩义)[1,2], Bing Duan(段冰)[1,2], Ying-Zhan Yan(严英占)[4], Yu Wu(吴宇)[5], Xiao-Chong Yu(俞骁翀)[6,7,†], Bei-Bei Li(李贝贝)[3,‡], and Da-Quan Yang(杨大全)[1,2,§]

[1] *State Key Laboratory of Information Photonics and Optical Communications, Beijing University of Posts and Telecommunications, Beijing* 100876, *China*
[2] *School of Information and Communication Engineering, Beijing University of Posts and Telecommunications, Beijing* 100876, *China*
[3] *Beijing National Laboratory for Condensed Matter Physics, Institute of Physics, Chinese Academy of Sciences, Beijing* 100190, *China*
[4] *Information Science Research Institute, China Electronics Technology Group Corporation, Beijing* 100876, *China*
[5] *The Key Laboratory of Optical Fiber Sensing and Communications (Education Ministry of China), University of Electronic Science and Technology of China, Chengdu* 610054, *China*
[6] *Department of Physics and Applied Optics Beijing Area Major Laboratory, Beijing Normal University, Beijing* 100875, *China*
[7] *School of Physics and Astronomy, Applied Optics Beijing Area Major Laboratory, Key Laboratory of Multiscale Spin Physics, Ministry of Education, Beijing Normal University, Beijing* 100875, *China*

(Received 28 April 2025; revised manuscript received 16 June 2025; accepted manuscript online 1 July 2025)

The enhancement of the microcavity quality factor contributes to fundamental linewidth reduction in microcavity lasers. This study demonstrates silica microrod resonators with quality factors approaching 10^9, fabricated by CO_2 laser reflow technology. To improve practical applicability, low-loss package techniques were developed, yielding packaged resonators with optimized optical performance. Using this platform, stimulated Raman lasing was achieved with a pump mode Q-factor of 1.333×10^9, exhibiting a threshold of 0.765 mW. The laser output stability was characterized by a standard deviation of 0.671 mV over 45 minutes of operation, with corresponding Allan deviation analysis. At the maximum output power of 106.4 μW, the measured frequency noise spectral density reached 0.46 Hz^2/Hz, corresponding to a linewidth of 2.89 Hz. Thermal tuning of the packaged module achieved a wavelength shift of 0.206 nm, with a temperature sensitivity of 8.92 pm/°C. This work establishes a new technical pathway for developing compact narrow-linewidth lasers, showing significant potential for medical diagnostics, optical communications, and defense applications.

Keywords: Raman laser, resonator, nonlinear optics, optical elements and devices

PACS: 42.55.–f, 42.60.Da, 42.65.-k, 42.79.–e

DOI: 10.1088/1674-1056/adea5a **CSTR:** 32038.14.CPB.adea5a

1. Introduction

Narrow-linewidth lasers, owing to their low phase noise and long coherence length, play a critical role in cutting-edge applications such as coherent optical communication, quantum communication, precision metrology, gravitational wave detection, and high-resolution imaging.[1–5] Whispering gallery mode (WGM) optical microcavities, characterized by their high quality (Q) factor and small mode volume, have emerged as ideal optical platforms for realizing low-threshold and narrow-linewidth lasers.[6]

In general, increasing the quality factor of a microcavity resonator can significantly reduce the Schawlow–Townes (ST) linewidth of the laser.[7] However, conventional microcavity lasers typically achieve lasing by integrating specific gain materials, such as rare-earth ions, organic dyes, or quantum dots, with silica microresonators.[8–11] For instance, in 2003, Vahala demonstrated laser emission at 1540 nm from a silica microsphere coated with an Er^{3+}-doped sol–gel thin film.[12] Later, Fan improved the doping process of rare-earth ions in the sol–gel method, successfully fabricating an Er^{3+}-doped silica microbubble cavity with a Q-factor as high as 5.2×10^7. They also achieved a tuning range of 4.4 nm through an all-optical tuning mechanism.[13] Although this approach enhances the Q-factor of doped microcavities, it remains at least an order of magnitude lower than that of undoped counterparts, which hinders further narrowing of the laser linewidth.

Microcavity lasers based on nonlinear optical effects offer a promising alternative to circumvent this limitation. Stimulated Raman scattering (SRS) and stimulated Brillouin scattering (SBS) are representative third-order nonlinear effects. SRS arises from the interaction between pump photons and optical phonons, while SBS involves interactions between pump photons and acoustic phonons.[14,15] Com-

†Corresponding author. E-mail: ydq@bupt.edu.cn
‡Corresponding author. E-mail: libeibei@iphy.ac.cn
§Corresponding author. E-mail: yuxc@bnu.edu.cn

© 2025 Chinese Physical Society and IOP Publishing Ltd. All rights, including for text and data mining, AI training, and similar technologies, are reserved.

pared to SBS, SRS generates Stokes light with a larger frequency shift, which helps extend the wavelength range of existing light sources.[16] To date, researchers have realized stimulated Brillouin lasers (SBLs) with sub-Hertz fundamental linewidths in silicon nitride microcavities,[17–19] silica microtoroid resonators,[19] silica microdisk resonators,[21,22] and silica microrod resonators.[23] In contrast, narrow-linewidth stimulated Raman lasers (SRLs) based on high-Q WGM microcavities have been rarely reported. For example, Lu achieved a Raman laser with a linewidth of 3 Hz in an SiO_2 microtoroid resonator.[24] Bao demonstrated a Raman laser in a crystalline AlN-on-sapphire microcavity with a Q-factor of 3.6×10^6. This laser exhibited a threshold of 8.3 mW and a frequency noise of 4.6 Hz^2/Hz, corresponding to a linewidth of 29 Hz.[25]

2. SRL linewidth theory

The fundamental linewidth of the SRL $\Delta\nu_{ST}$ can be described as follows:[24,26]

$$\Delta\nu_{ST} = \left(1+\alpha^2\right)\frac{2\pi\left(1+K_Q\right)K_Q\hbar\nu^3}{PQ_0^2}, \tag{1}$$

Here, P denotes output power of the SRL, $\hbar$ is the reduced Planck constant, ν is the SRL frequency, and α describes the phase fluctuation coupled from intra-cavity pump intensity fluctuation due to the Kerr nonlinearity. Moreover, Q_0 represents the intrinsic quality factor of the optical resonance mode associated with the SRL, while Q_e is the coupling-related quality factor. These parameters satisfy the relation $K_Q = Q_0/Q_e$. Equation (1) shows that the fundamental linewidth of the SRL is inversely proportional to the square of the microcavity Q-factor, implying that high-Q microcavities enable the generation of narrow-linewidth SRLs.

2.1. Fabrication

Figure 1(a) shows our automated system for fabricating silica microrod resonators through CO_2 laser reflow technology. The fabrication process utilizes a high-purity quartz preform rod with a diameter of 3 mm. Prior to processing, the preform rod is sectioned into predetermined lengths and rigidly mounted on a computer-controlled translational spindle using a mechanical chuck assembly. The spindle rotates at a constant angular velocity of 600 rpm to ensure uniform surface heating during laser micromachining. The CO_2 laser output power (maximum 75 W) is modulated by pulse-width modulation using an arbitrary function generator (AFG), while the duty cycle is adjusted through computer control. The laser beam is then focused through a ZnSe lens onto the preform rod. In the laser interaction zone, silica undergoes localized melting and ablation. Under surface tension, the molten material redistributes laterally, forming a groove structure.[27] First, bilateral grooves are fabricated by high-power (70% duty cycle) laser micromachining, constructing the foundational microcavity structure. Subsequently, the laser power is reduced to 30% duty cycle, and a stepper motor moves the preform rod at 2 mm/min, enabling bidirectional laser scanning between the grooves. This process will create a whispering gallery region with smooth surface and uniform roundness.[28] Finally, multiple laser reflow cycles are performed at 20% duty cycle to achieve both surface quality enhancement and precise geometric control of the microcavity.

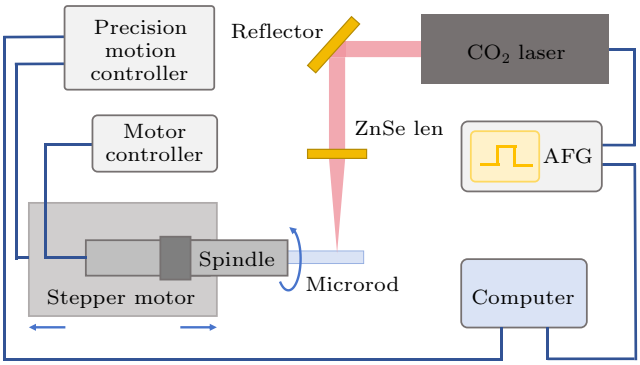


Fig. 1. The automated preparation system for silica microrod cavities. AFG: arbitrary function generator.

Figure 2(a) displays a fabricated silica microrod resonator. For optical characterization of the resonator, we statistically analyzed the quality-factor distribution of resonant modes within one free spectral range (FSR). As shown in Fig. 2(b), 21 resonant modes possess Q-factors above 10^9, with the highest Q-factor reaching 2.3×10^9. Furthermore, utilizing these optimized processing parameters in the automated fabrication setup enables reproducible production of microrod resonators with ultrahigh Q-factors.

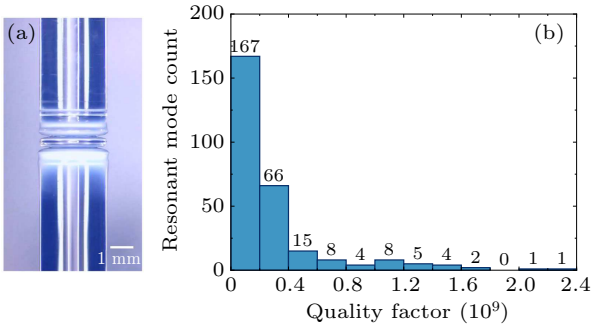


Fig. 2. Characterization of the microrod resonator: (a) optical microscope image of the microrod resonator, (b) Q-factor distribution of resonant modes within one FSR of the microrod resonator.

Despite their excellent optical performance, the practical application of microrod resonators faces significant challenges, including intricate coupling requirements, high sensitivity to environmental disturbances, and limited operational stability over extended periods. To address these issues, we developed a miniaturized and environmentally stable packaged resonator module. As illustrated in Fig. 3(a), the module features a dual-layer aluminum alloy architecture comprising inner and outer enclosures. The microrod resonator is fixed at

the central groove of the inner enclosure using UV-curable adhesive. The fiber taper, which couples to the microrod resonator, is also secured to the sidewalls of both the inner and outer enclosures using low-loss UV-curable adhesive. The thermal control system consists of a thermistor and a thermoelectric cooler (TEC). The gap between the inner and outer enclosure is filled with thermal conductive silicone, which enhances the mechanical stability of the module and facilitates efficient thermal transfer between the TEC and the inner enclosure. To further isolate the resonator from the external environment, the gaps between the sidewalls and the lid of the outer enclosure were sealed with UV-curable adhesive.

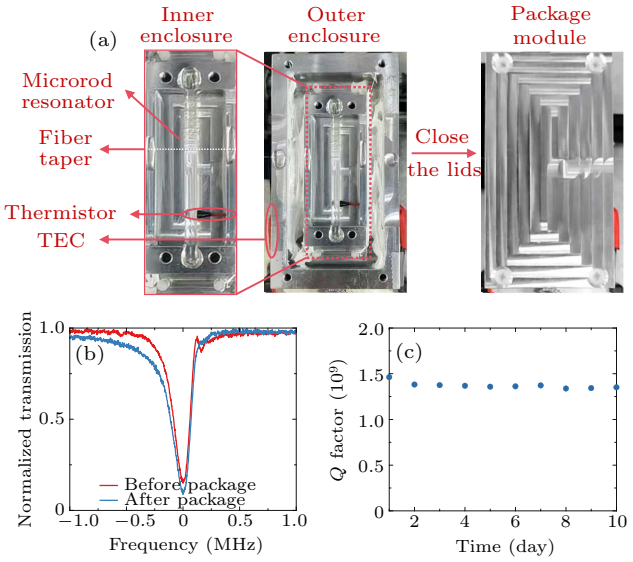


Fig. 3. Package module and performance characterization: (a) structural diagram of package module, (b) transmission spectrum of the same mode before and after packaging, (c) the Q-factor stability within 10 days.

Figure 3(b) presents the transmission spectrum of the same resonant mode acquired before and after packaging under the identical frequency-scanning rate. Prior to packaging, the resonant mode exhibited a narrower linewidth, along with an observable ringdown effect. To ensure accurate Q-factor measurements, the scanning speed was reduced to suppress the ringdown effect,[29] yielding a calculated Q-factor of 1.507×10^9. After packaging, the mode's linewidth broadened, and the ringdown phenomenon disappeared, resulting in a measured Q-factor of 1.445×10^9. These results demonstrate that despite introducing additional optical losses during packaging, the encapsulated module retains a high Q-factor. The variation of the Q-factor in the packaged module over a 10-day period was measured, as shown in Fig. 3(c). A noticeable reduction in the Q-factor was observed on the second day after packaging, attributed to the adsorption of water molecules from ambient air onto the silica microcavity surface, which increased optical dissipation.[30] Thereafter, the Q-factor stabilized, suggesting that the surface hydroxyl group may have reached saturation, allowing the packaged module to maintain a relatively stable Q-factor in the subsequent days.

2.2. Experiment

Figure 4 illustrates the experimental setup for SRL generation and characterization based on the packaged microrod resonator. The transmission signal from the microrod resonator is monitored by oscilloscope (OSC1) and fed back to a servo to achieve laser frequency locking.[31] A Raman wavelength-division multiplexer (RWDM) separates and outputs laser signals at 1450 nm, 1550 nm, and 1660 nm, thereby extracting the purified SRL. The single-sideband (SSB) frequency noise of the SRL is measured using the self-heterodyne method.[32–34] The generated SRL is first directed into an acousto-optic modulator (AOM, Brimrose), which splits the beam into two paths: the 0th-order light enters a 10-km fiber delay line, while the 1st-order light (55-MHz frequency shift) passes through a polarization controller. The two beams are then recombined at a coupler and detected by a photodetector to generate a beat signal, which is recorded by a digital oscilloscope (OSC2). The recorded beat signal is processed via Hilbert transform (HT), fast Fourier transform (FFT), and compensation algorithms to retrieve the single-sideband (SSB) frequency noise power spectral density (PSD) of the SRL.[35] Typically, the frequency noise PSD comprises $1/f$ noise at low offset frequencies and white noise at higher frequencies.[36] In the low-frequency region, the noise power decreases with increasing offset frequency, while in the high-frequency region, it flattens out, exhibiting white-noise behavior. Assuming the observed white noise level in the high-frequency region is S_v, the laser linewidth $\Delta\nu$ can be approximated as $\Delta\nu = 2\pi S_v$.

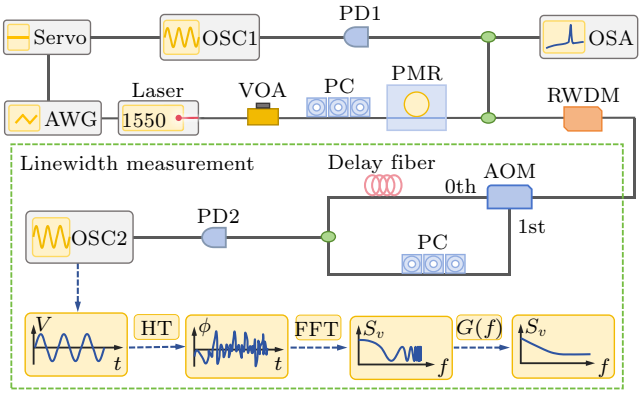


Fig. 4. Experimental setup, AWG: arbitrary waveform generator; OSC: oscilloscope; VOA: variable optical attenuator; PC: polarization controller; PMR: packaged microrod resonator; OSA: optical spectrum analyzer; RWDM: Raman wavelength division multiplexer; AOM: acoustic-optic modulator; PD: photodetector; HT: Hilbert transform; FFT: fast Fourier transform; $G(f)$: compensation function.

As illustrated in Fig. 5(a), the packaged module was characterized using a Mach–Zehnder interferometer (MZI) with a 14.551-MHz FSR, yielding an intrinsic Q-factor of 1.333×10^9 for the pump mode. The optical spectrum of the SRL is shown in Fig. 5(b). The pump laser exhibited a center wavelength of 1552.644 nm, while the SRL emission was centered

at 1646.932 nm, corresponding to a Stokes shift of approximately 11.06 THz. Additionally, multiple sideband peaks with a frequency spacing of 17.2 GHz were observed near the pump laser, originating from four-wave mixing (FWM) effect.

Figure 5(c) demonstrates the dependence of the SRL output power on the pump power, with the latter controlled by a variable optical attenuator (VOA). A fit to the data reveals the threshold power of approximately 0.765 mW. To evaluate the output stability, the SRL was directed into the photodetector, which converted the optical signal into an electrical output signal. This output signal was continuously monitored for 45 minutes using a data acquisition card at a sampling rate of 10 Hz. The top panel of Fig. 5(d) shows the recorded output signal, with a calculated standard deviation of 0.671 mV. The Allan variance of the laser output is also shown in the bottom panel of Fig. 5(d). The Allan variance of the SRL output signal is relatively small, exhibiting values on the order of 10^{-2} over short timescales (< 1 min), and approximately 10^{-1} over longer timescales (1 min to 10 min).

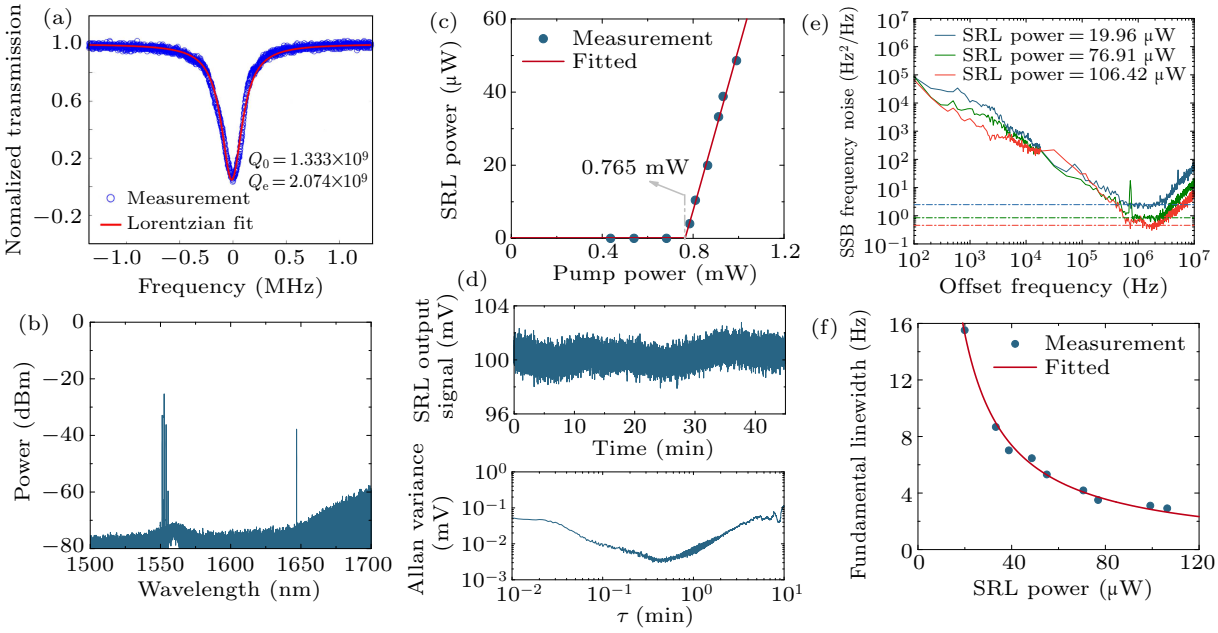


Fig. 5. Characterization of Raman laser. (a) Transmission measurement of the pump mode. (b) Optical spectra of SRL. (c) SRL power *versus* pump power. (d) SRL output signal (top) and Allan variance (bottom). (e) SSB frequency noise spectra of SRL at different powers. (f) Fundamental linewidth of SRL with different powers.

Additionally, we measured the frequency noise of the SRL under different output power conditions. Figure 5(e) characterizes the SSB frequency noise PSD of the SRL, where the plateau region at higher offset frequencies corresponds to the white noise. The observed white noise level exhibits reduction with increasing laser output power. When the SRL reaches its maximum output power of 106.4 μW, the average white noise level observed is approximately 0.46 $\mathrm{Hz^2/Hz}$, corresponding to a minimum laser linewidth of 2.89 Hz. Figure 5(f) illustrates the variation of the SRL linewidth as a function of output power. The fitting results demonstrate an inverse relationship between fundamental linewidth and output power, in good agreement with Eq. (1).

Thermal tuning is one of the primary methods for tuning WGM microresonator lasers due to its excellent reversibility and wide tuning range. The fundamental principle is that changes in the ambient temperature surrounding the resonator cause variations in both the cavity's physical dimensions and the refractive index of the material, resulting in a shift in the resonant wavelength. In a WGM microcavity, the temperature dependence of the resonant wavelength can be expressed as

$$\frac{\mathrm{d}\lambda}{\mathrm{d}T} = \lambda_0(\alpha+\beta), \tag{2}$$

Here, λ_0 denotes the initial resonant wavelength, α is the thermo-optic coefficient, and β represents the thermal expansion coefficient. Since silica has both a positive thermo-optic coefficient and a positive thermal expansion coefficient, the resonant modes of the silica resonator will shift toward longer wavelengths as the temperature increases.[37,38]

During the experiment, the target temperature was set using a TEC temperature controller, forming a closed-loop feedback system with a high-sensitivity thermistor and the TEC to precisely regulate the temperature of the packaged module, as shown in Fig. 6. In the thermal tuning experiment of the SRL, the temperature of the packaged module was sequentially set to nine values: 17.6 °C, 21.2 °C, 24.4 °C, 27.1 °C, 30.4 °C, 32.8 °C, 35.5 °C, 38.1 °C, and 40.6 °C. As the temperature increased, the resonant modes of the resonator exhibited a redshift, requiring real-time adjustment of the bias voltage of the sweep signal to track the shifted resonance. The

successful reappearance of a stable Raman laser signal on the optical spectrum analyzer (OSA) confirmed the completion of laser tuning. Figure 6(a) shows the output wavelength of the pump laser tuned at different temperatures, while figure 6(b) presents the corresponding SRL excited by the pump. Experimental results show that, as the module temperature increased from 17.6 °C to 40.6 °C, the laser wavelength was continuously tuned over a range of 0.206 nm, corresponding to a wavelength–temperature tuning coefficient of 8.92 pm/°C.

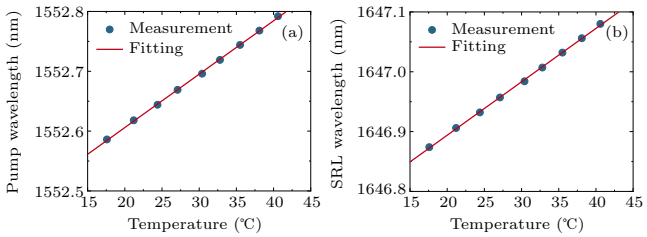


Fig. 6. Experimental results of thermal tuning: (a) pump wavelength at different temperatures, (b) variation of SRL wavelength with respect to temperature.

3. Conclusion

This study demonstrates a tunable narrow-linewidth Raman laser based on a packaged high-Q silica microrod resonator. The linewidth of this Raman laser can be narrowed to 2.89 Hz, surpassing the previous 3-Hz record linewidth demonstrated in Ref. [24]. Furthermore, the microcavity-fiber taper coupling system presented in Ref. [24] was exposed to ambient air, making it susceptible to degradation from water molecules, contaminants, and external disturbances, which can adversely affect the resonator's Q-factor and laser output stability.[39] In contrast, we have incorporated a low-loss packaging technique. This approach consolidates the bulky fiber-coupling setup into a compact and robust enclosure for practical deployment, while simultaneously isolating the system from the external environment. The packaged module maintains a Q-factor on the order of 10^9 over a 10-day period. An integrated temperature control system stabilizes the resonator's ambient temperature to ensure stable laser output and enables wavelength tunability. The laser demonstrated high stability with an output standard deviation of 0.671 mV over 45 minutes and the continuous wavelength tuning of approximately 0.206 nm. Additionally, compared to microtoroid resonators used in Ref. [24], microrod resonators exhibit a simpler fabrication process and lower cost. Significantly, the Raman laser enables access to the underutilized U-band (1625 nm–1675 nm). This facilitates coexistence with C+L-band systems, thereby expanding optical fiber capacity without infrastructure modification. Furthermore, with its linewidth on the order of Hertz, the laser suppresses phase noise *versus* commercial DFB lasers, permitting higher order quadrature amplitude modulation for single-channel bitrate enhancement.[40,41] The narrow-linewidth laser is promising for high-precision gas sensing like acetylene (C_2H_2) monitoring, as its high spectral purity resolves closely spaced absorption lines.[42,43] In conclusion, the Raman laser combines low cost, narrow linewidth, high stability, and tunability, offering application potential in diverse fields such as precision metrology, optical communications, quantum optics, and high-resolution sensing.

Acknowledgements

Project supported by the National Natural Science Foundation of China (Grant Nos. 12474372, 12474429, 62222515, and 12174438), the National Key Research and Development Program of China (Grant Nos. 2023YFB2805600 and 2023YFB2806200), the Natural Science Foundation of Beijing Municipality (Grant No. Z210004), and the Fund from the State Key Laboratory of Information Photonics and Optical Communications (Grant No. IPOC2024ZR01).

References

[1] Hu J, Wang W, Xie Z Y, Liu C N, Li F and Yang D Q 2024 *Photon. Res.* **12** 2573
[2] Yang Q, Li Y, Zou H, Mei J, Xu E M and Zhang Z X 2024 *Chin. Phys. B* **33** 024206
[3] Lang X K, Jia P, Chen Y Y, Qin L, Liang L, Chen C, Wang Y B, Shan X N, Ning Y Q and Wang L J 2019 *Sci. China Inf. Sci.* **62** 19203
[4] Duan B, Zhou H Y, Chen J H, Ma C H, Zhao X Y, Zheng X L, Wang C, Liu L and Yang D Q 2022 *Photon. Res.* **10** 2343
[5] Chen S Y, Deng H Q, Zhang W R, Dai Y P, Wang T, Yu Q, Li C, Jiang M, Su R T and Wu J 2023 *Chin. Phys. B* **32** 074203
[6] Duan B, Zhang X, Yu X C, Zhao Y X, Chen J H, Gao Y P, Wang C and Yang D Q 2025 *Photon. Sens.* **15** 250310
[7] Schawlow A L and Townes C H 1958 *Phys. Rev.* **112** 1940
[8] Wang J, Zhan T R, Huang G S, Chu P K and Mei Y F 2014 *Laser Photon. Rev.* **8** 521
[9] Javerzac-Galy C, Kumar A, Schilling R D, Piro N, Khorasani S, Barbone M, Goykhman L, Khurgin J B, Ferrari A C and Kippenberg T J 2018 *Nano Lett.* **18** 3138
[10] Reed J C, Zhu A Y, Zhu H, Yi F and Cubukcu E 2015 *Nano Lett.* **15** 1967
[11] Grivas C, Li C Y, Andreakou P, Wang P F, Ding M, Brambilla G, Manna L and Lagoudakis P 2013 *Nat. Commun.* **4** 2376
[12] Cai M, Painter O, Vahala K J and Sercel P C 2000 *Opt. Lett.* **25** 1430
[13] Zhu S, Shi L, Xiao B W, Zhang X L and Fan X D 2018 *ACS Photon.* **5** 3794
[14] Zhu S, Xiao B W, Jiang B, Shi L and Zhang X L 2019 *Nanophotonics* **8** 931
[15] Tian J Y and Lin G P 2023 *J. Lightwave Technol.* **42** 2118
[16] Spillane S M, Kippenberg T J and Vahala K J 2002 *Nature* **415** 621
[17] Liu K K and Blumenthal D J 2024 *Conference on Lasers and Electro-Optics (CLEO)*, May 5–10, 2024, Charlotte, USA, pp. 1–2
[18] Gundavarapu S, Brodnik G M, Puckett M, Huffman T, Bose D, Behunin R, Wu J F, Qiu T Q, Pinho C, Chauhan N, Nohava J, Rakich P T, Nelson K D, Salit M and Blumenthal D J 2019 *Nat. Photon.* **13** 60
[19] Liu K K, Wang J W, Chauhan N, Harrington M W, Nelson K D and Blumenthal D J 2023 *Opt. Lett.* **49** 45
[20] Qin Y C, Ding S L, Zhang M H, Wang Y N, Shi Q, Li Z X, Wen J M, Xiao M and Jiang X S 2022 *Opt. Lett.* **47** 1638
[21] Yuan Z Q, Wang H M, Wu L, Gao M D and Vahala K J 2020 *Optica* **7** 1150
[22] Li J, Lee H, Chen T and Vahala K J 2012 *Opt. Express* **20** 20170
[23] Wang M, Liu C N, Zhou X, Li J C, Wang Z, Yang D Q, Yang Q F and Li B B 2025 *ACS Photon.* **12** 2318

[24] Lu T, Yang L, Carmon T and Min B 2011 *IEEE J. Quantum Electron.* **47** 320
[25] Liu K W, Yao S Y, Ding Y L, Wang Z H, Guo Y N, Yan J C, Wang J X, Yang C X and Bao C Y 2022 *Opt. Lett.* **47** 4295
[26] Roos P A, Murphy S K, Meng L S, Carlsten J L, Ralph T C, White A G and Brasseur J K 2003 *Phys. Rev. A* **68** 013802
[27] Del'Haye P, Diddams S A and Papp S B 2013 *Appl. Phys. Lett.* **102** 221119
[28] Yang D Q, Guo Y Y, Chen W, Wu Y R, Zhai K P and Wang X 2022 *J. Lightwave Technol.* **41** 1768
[29] Chen Y, Zhou Z H, Zou C L, Shen Z, Guo G C and Dong C H 2017 *Opt. Express* **25** 16879
[30] Jager J B, Calvo V, Delamadeleine E, Hadji E, Noé P, Ricart T, Bucci D and Morand A 2011 *Appl. Phys. Lett.* **99** 181123
[31] Wang H, Duan B, Wang K, Wu X Y, Gao Y P, Lu B, Yang D Q and Wang C 2023 *Nanophotonics* **12** 3757
[32] Cui M B, Huang J G and Yang X L 2021 *Laser Optoelectron. Prog.* **58** 0900005
[33] Yuan Z Q, Wang H M, Liu P, Li B H, Shen B Q, Gao M D, Chang L, Jin W, Feshali A, Paniccia M, Bowers J and Vahala K J 2022 *Opt. Express* **30** 25147
[34] Chen J Q, Chen C, Sun J J, Zhang J W, Liu Z H, Qin L, Ning Y Q and Wang L J 2024 *Sensors* **24** 3656
[35] Exter M P V, Kuppens S J M and Woerdman J P 1992 *IEEE J. Quantum Electron.* **28** 580
[36] Domenico G D, Schilt S and Thomann P 2010 *Appl. Opt.* **49** 4801
[37] Wu Y R, Duan B, Song J E, Liu X, Yu X C, Wang C and Yang D Q 2023 *Opt. Express* **31** 18851
[38] Song R, Zhang X, Feng S, Liu S Y, Duan B and Yang D Q 2024 *Results Phys.* **2** 107806
[39] Gao Y, Liu T, Wang S Y and Guo H R 2022 *Infrared Laser Eng.* **51** 20220294 (in Chinese)
[40] Shimizu S, Takayuki K, Akira K, Takushi K, Masanori N, Koji E, Takahiro K, Masashi A, Takeshi U, Yutaka M, Tomoyuki K, Yu T and Takeshi H 2024 *J. Lightwave Technol.* **42** 1347
[41] Xu F, Qiao Y, Zhou J, Guo M Q and Tian H P 2017 *Opt. Fiber Technol.* **34** 36
[42] Gordon I E, Rothman L S, Hargreaves R J, *et al.* 2022 *J. Quant. Spectrosc. Radiat. Transf.* **277** 107949
[43] Hodgkinson J and Tatam R P 2012 *Meas. Sci. Technol.* **24** 012004